Looking inside an endohedral fullerene: Inter- and intramolecular ordering of Dy3N@C80 (Ih) on Cu(111)

Treier, M ; Ruffieux, P ; Fasel, R ; Nolting, F ; Yang, S ; Dunsch, L ; Greber, T

DOI: https://doi.org/10.1103/PhysRevB.80.081403

Looking inside an endohedral fullerene: Inter- and intramolecular ordering of $Dy_3N@C_{80}$ (I_h) on Cu(111)

Matthias Treier[1], Pascal Ruffieux[1], Roman Fasel[1], Frithjof Nolting[2], Shangfeng Yang[3,4], Lothar Dunsch[3], Thomas Greber[5]*

[1] Empa, Swiss Federal Laboratories for Materials Testing and Research, nanotech@surfaces Laboratory, 3602 Thun and 8600 Dübendorf, Switzerland

[2] Swiss Light Source, Paul Scherrer Institut, 5232 Villigen PSI, Switzerland

[3] Leibniz Institute for Solid State and Materials Research, Dresden, Germany

[4] Hefei National Laboratory for Physical Sciences at Microscale and Department of Materials Science and Engineering, University of Science and Technology of China, Hefei 230026, China

[5] Physics Institute, University of Zurich, 8057 Zurich, Switzerland

* to whom correspondence should be addressed: matthias.treier@gmail.com

PACS: *61.05.js X-ray photoelectron diffraction; 68.35.bp Fullerenes;* 68.37.Ef Scanning tunneling microscopy; 68.43.Fg Adsorbate structure (binding sites, geometry); 61.48.-c Structure of fullerenes and related hollow molecular clusters

Abstract

The inter- and intramolecular ordering of the trimetallic nitride endohedral fullerene $Dy_3N@C_{80}$ with icosahedral cage symmetry I_h on Cu(111) has been studied by scanning tunneling microscopy (STM) and synchrotron-based X-ray photoelectron diffraction (XPD). $Dy_3N@C_{80}$ (I_h) is found to form ordered islands consisting of domains of equally oriented molecules. As for C_{60} on the same substrate, the cage is facing with a hexagon towards the surface which is however slightly tilted for C_{80}. The endohedral nitrogen atom remains at a position close to the geometrical center of the cage. Resonant XPD on the M_V edge shows that the encaged Dy_3N unit takes well-defined orientations with respect to the C_{80} cage and the Cu(111) substrate.

Metal-containing endohedral fullerenes have attracted great interest over the last decade due to their unique electronic properties associated with the charge transfer from the endohedral metal complex to the carbon cage. Endohedral fullerenes exhibit a variety of novel properties such as peculiar redox- and electrochemical behavior, luminescence and nonlinear optical response [1]. Furthermore, they represent an interesting class of materials since they offer the opportunity to study and possibly manipulate small clusters of endohedral atoms which might for example be applied in future information storage devices. Due to the comparably high production yields that can be achieved, research on endohedral trimetallic nitride cluster (TNT) fullerenes [2, 3] has increased in recent years [2, 4-7]. TNT endohedral fullerenes have been shown to possess an endohedral ordering in condensed phases such as co-crystals [5, 8]. They have also been shown to possess unique magnetic properties [7, 9], motivating their application in future memory storage devices. For such applications, ordered arrays of endohedral units and the possibility to switch the orientation of the endohedral units to store information are required. The self-assembly of TNT endohedral fullerenes on surfaces has been analyzed previously by Scanning tunneling microscopy (STM) [10-12]. However, these studies have not addressed the issue of endohedral ordering in the adsorbed state since this information is not accessible by STM studies alone. On the other hand, the position of the metal atom with respect to the cage of single-atom endohedral metallofullerenes has been studied by X-ray standing wave techniques [13, 14], without however simultaneously addressing the orientation of the cage.

In this letter we present a detailed study of (sub-)monolayers of the endohedral trimetallic nitride cluster fullerene $Dy_3N@C_{80}$ (I_h) [6] on Cu(111) (see Fig. 1). We show that the combination of STM and both standard and resonant X-ray photoelectron diffraction (XPD) allows for a determination of the inter- and intramolecular ordering. The application of XPD unravels for the first time the arrangement of an endohedral unit on a surface. We find that $Dy_3N@C_{80}$ (I_h) forms an ordered superstructure on this template, with both the cage and the endohedral unit being ordered with respect to the substrate.

Angle-scanned X-ray photoelectron diffraction experiments were performed at the NearNode-endstation of the SIM beamline at the Swiss Light Source. Low temperature STM (LT-STM) measurements were conducted using an Omicron LT-STM. Both systems were operated at ultra high vacuum conditions with base pressure below 2×10^{-10} mbar. $Dy_3N@C_{80}$ (I_h) has been deposited from resistively heated quartz / diamond-like carbon coated steel crucibles held at about 770 K onto the sample which was held at room temperature. The substrate has been cleaned by standard Ar^+-ion sputtering / annealing cycles prior to deposition of the endohedral fullerene. XPD has been performed at room temperature while STM data was acquired at 77 K.

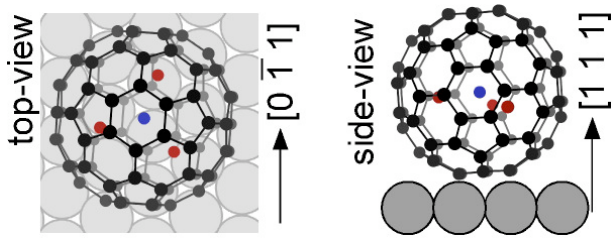

Figure 1: Model of $Dy_3N@C_{80}$ (I_h) adsorbed on Cu(111). Carbon atoms are shown in greyscale while red/blue atoms correspond to endohedral dysprosium/nitrogen atoms.

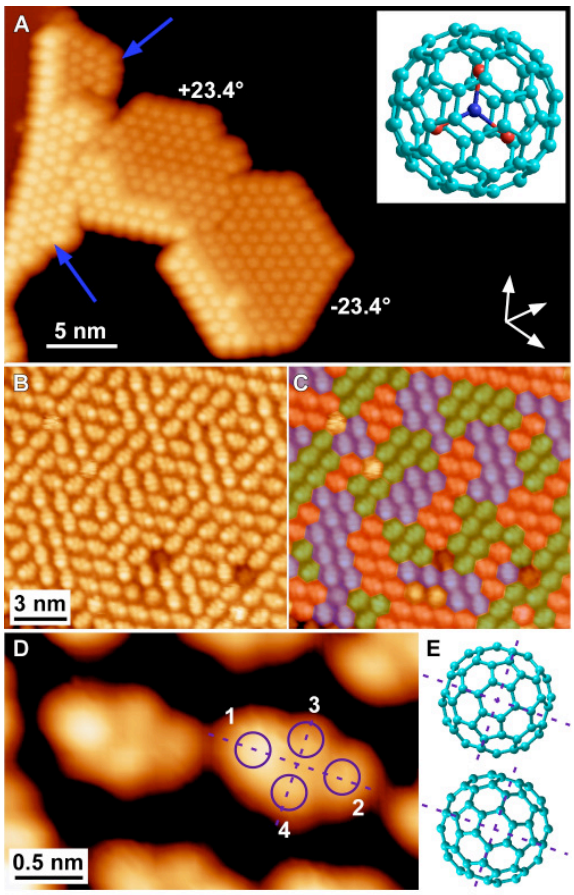

Figure 2: STM images of $Dy_3N@C_{80}$ (I_h) on Cu(111). (A) Overview image showing the correlation between the overlayer structure and the local step edge direction. Blue arrows point to small patches of adsorbates which adopt a superstructure different from the dominant $\sqrt{19}$ superstructure. (B) Intramolecular contrast resolved STM image of a +23.4° island showing the formation of small domains of equally oriented molecules within an island. (C) Visualization of domains; coloured STM image of the area shown in (B). (D) High resolution STM image of two molecules, showing intramolecular contrast. Four protrusions per molecule can be identified. (E) Suggested models of C_{80} cage orientation compatible with the symmetry of the intramolecular features from (D). Dashed lines correspond to the symmetry elements from (D). (Scanning parameters: (A) 80 pA, -1.8 V (B,C,D) 0.3 nA, -0.1 V).

STM measurements [15] of submonolayers of $Dy_3N@C_{80}$ (I_h) on Cu(111) show that islands of the adsorbate grow out from step edges on both the lower and upper terrace adjacent to the step. Locally, the orientation of the superstructures follows the orientation of the step edges as shown in Figure 2a. However, low energy electron diffraction (LEED) shows that at higher coverage (close to a complete monolayer), a $(\sqrt{19}\times\sqrt{19})R\pm 23.4°$ dominates with no other superstructures spanning over dimensions to be visible in LEED. The nearest neighbor distances in the other superstructures are – within the measurement error of STM - equal to the ones within the long-range ordered superstructure (1.1 nm). High resolution STM images show that within islands of the $\sqrt{19}$ superstructure, three rotationally equivalent molecular orientations are found. Equally oriented molecules form small domains of typically 5-15 molecules within larger islands as shown in Figures 2b&c.

A high resolution image with clearly resolved intramolecular structure is shown in Figure 2d. Four protrusions per molecule can be discerned. While the protrusions labeled 3 and 4 approximately have the same apparent height, this is not the case for protrusions 1 and 2, with protrusion 1 appearing 0.2-0.3 Å higher. The particular intramolecular contrast cannot be readily related to a molecular orbital or structural elements of the cage. However, it is possible to derive possible adsorption orientations of the cage based on symmetry considerations. The molecule appears to be symmetric with respect to the dashed lines passing through maxima 1 and 2 (Figure 2d) while the difference in apparent height can be explained by a rotation of the cage around the axis represented by the dashed line passing through maxima 3 and 4. Such a rotation would correspond to a tilt of the cage with respect to a highly symmetric adsorption geometry. Two adsorption geometries compatible with these symmetry considerations are given in Figure 1e with the cage facing toward the surface with a hexagon in both cases. Since electronic and geometric effects cannot be clearly separated by STM, a quantitative analysis of this tilt and unambiguous determination of the adsorption geometry is not possible by STM alone. In particular, STM does not yield information on the endohedral ordering. We have therefore complemented the STM results by an XPD study, a combination of techniques which has previously been shown to allow for a determination of the three-dimensional orientation of large organic adsorbates [16].

C1s- and N1s-XPD patterns are shown in Figures 3a&c. The C1s-XPD pattern (Figure 3a) of a monolayer of $Dy_3N@C_{80}$ (I_h) bears some resemblance to the corresponding pattern produced by a monolayer of C_{60} on the same substrate [17]. However, the pattern produced by the C_{80} cage is rotated azimuthally by 30° compared to the case of C_{60}, directly indicting that the adsorption orientation must be different for this type of fullerene. The large number of inequivalent emitter-scatterer directions is directly

reflected in the broad shape of the maxima. Due to the single photoelectron emitter per molecule, the N1s photoelectron diffraction pattern (Figure 3c) is highly anisotropic (~20%). It is therefore possible to measure clearly distinguishable diffraction features even at this low nitrogen concentration of only about ~1 atom/nm^2 within the $Dy_3N@C_{80}$ (I_h) monolayer. Single scattering cluster (SSC) simulations [18] have been used to find the molecular orientation yielding the lowest reliability factor (*R*-factor) and hence the best agreement with experiment [19]. Backscattering from substrate atoms has been neglected since the backscattering yield is very low within the kinetic energy range used for this work (> 400 eV).

From both the C1s- and the N1s-XPD patterns, it is found that, similar to C_{60}, the C_{80} cage is facing towards the surface with a hexagon. However, the exact orientation of the hexagon in C_{80} differs from the one determined for C_{60}. As mentioned in the previous section, STM stipulates an out-of-plane rotation of the cage which is confirmed by XPD (see supporting information for details). The best fit with experiment is obtained for a tilt angle ψ of the hexagon face of 3°±2° with respect to the (111) plane of the substrate and an azimuthal orientation ϕ = 4°±2° which compares well with the STM result from which ϕ can be estimated to about 6°±6°. Figure 1 illustrates this best-fit orientation of the C_{80} cage. Only the cage orientation shown in the bottom part of Figure 2e is thus compatible with XPD. The alternative model derived from STM (upper part of Figure 2e) can be excluded based on the SSC analysis. We note that the *R*-factor has a shallow minimum around this adsorption configuration which is reflected in the relatively large error associated with the cage orientation. We have however also independently determined the cage orientation from the N1s-XPD data, and the same orientational angles were found to give the lowest *R*-factor, suggesting that the actual error is smaller than the value quoted above. The position of the endohedral nitrogen atom in the direction orthogonal to the surface has also been determined by SSC. It is found that the nitrogen atom remains at a position close to the centre of the C_{80}-cage also in the adsorbed state (Fig. 1). A pronounced minimum is found for a position of the nitrogen atom at 0.1±0.2 Å below the geometrical centre of the cage. As can be seen by comparing Figures 3a&b and 3c&d respectively, the agreement between simulated and measured diffraction patterns is excellent for both C1s and N1s patterns.

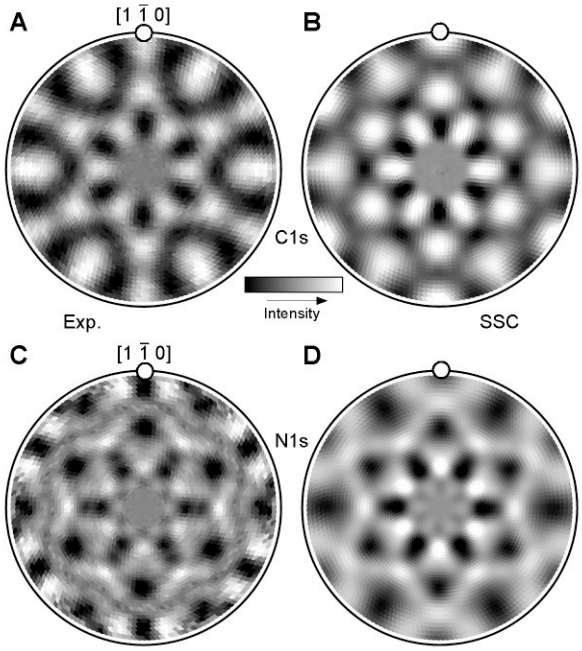

Figure 3: Synchrotron radiation (*hv*=880 eV) XPD study of 1ML of $Dy_3N@C_{80}$ (I_h) on Cu(111). (A) Experimental C1s-XPD (B) Best-fit C1s-SSC (C) Experimental N1s-XPD (D) Best-fit N1s-SSC.

While C1s and N1s photoelectron diffraction patterns of excellent quality could be measured by standard synchrotron-based angle-scanned XPD, similar recording of Dy4d patterns proved unsuccessful. The large number of final states leads to a significant broadening of the Dy4d peak [20] resulting in a low peak-to-background ratio. In conjunction with the strongly anisotropic secondary electron background (due to the close-lying Cu3s photoelectron peak) this prevents a clear assignment of diffraction features to Dy4d photoelectrons. In order to increase the peak-to-background ratio we used resonant x-ray photoelectron diffraction (rXPD) [21, 22]. Here this technique is exploited to enhance the signal-to-background ratio of Dy emitters. The signal at a given energy is proportional to the ratio between the cross section and the line width. As outlined above, the broad Dy4d multiplet inhibits the observation of off-resonance Dy4d XPD patterns, although the Dy4d photoemission cross section is significantly larger than that of N1s. Resonant excitation of the Dy3d-4f transition enhances the cross section to linewidth ratio by more than two orders of magnitude. As shown below, the angular modulation of the corresponding Auger electron emission allows for the acquisition of statistically significant Dy-related diffraction data.

The inset in Figure 4a shows the X-ray absorption spectrum of one monolayer of $Dy_3N@C_{80}$ (I_h) on Cu(111). It corresponds to that of trivalent Dy and peaks at about 1291 eV photon energy [23], where the *MN* absorption and subsequent electron emission with a kinetic energy of 1281 eV are highest. Figure 4a

shows the dependence of the electron emission intensity on the photon energy. The Cu3d substrate valence band emission remains constant and follows the photon energy, as does the resonant Dy-*MNN* emission at 1281 eV. This indicates that most of the emission is due to Auger resonant Raman deexcitation, where the photoexcited electron still resides on the Dy atom while it deexcites and not due to a regular Auger deexcitation that is independent of the photon energy [24]. However, both of these Auger emission processes are expected to have localized electron source waves that are a prerequisite for the interpretation of angle-scanned electron diffraction data, and we may thus make use of their greatly enhanced signal to background ratio.

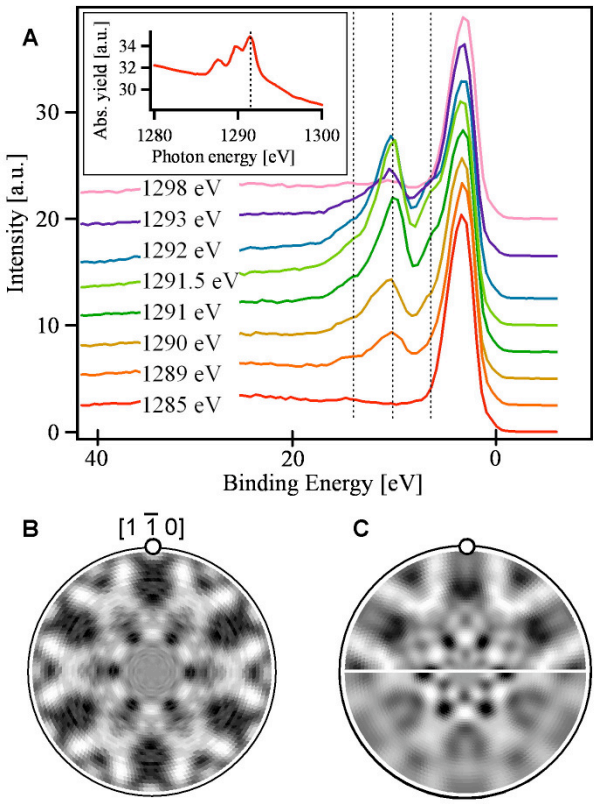

Figure 4: rXPD of Dy-*MNN* Auger lines. (A) Resonant enhancement of Auger lines (dotted lines) as a function of photon energy. The inset shows the corresponding X-ray absorption spectrum across the Dy M_V edge (3d). The dashed line designates the photon energy of 1291.5 eV. (B) Dy-*MNN*-rXPD of 1ML $Dy_3N@C_{80}$ (I_h) on Cu(111), recorded at a photon energy of 1291.5 eV. (C) Best-fit SSC simulation (upper half, see text for details) and simulation based on disordered endohedral unit (lower half).

Figure 4b shows a rXPD pattern recorded at a photon energy of 1291.5 eV on the strongest Dy-*MNN* Auger feature (central dashed line in Figure 4a). The ordering of the fullerene cages as evidenced by the data in Figure 3 also imposes a diffraction pattern with sizable contrast for Dy emitters that are randomly distributed on a sphere inside the carbon cage (see lower half of Figure 4c). The unsatisfactory R-factor and small anisotropy of this simulation do however clearly exclude this possibility. This infers that there exists order between the cage and the endohedral units. Further SSC simulations show that this endohedral ordering is different from the one found in bulk phases [8] (see supporting information). It must therefore be concluded that the endohedral Dy_3N unit "feels" the underlying Cu(111) surface and adopts suitable orientations.

To investigate further on the orientation of the endohedral Dy_3N unit, the experimental Dy-rXPD pattern has been compared to a series of SSC simulations based on different model systems, considering both planar and pyramidal endohedral units. A slight deviation from planarity in bulk crystals has been suggested in the literature [8], but smaller (<0.1 Å) than for other endohedral trimetallic nitride cluster fullerenes [5]. Details on the SSC simulations are given in the supporting information. To summarize these simulations, we find that a single orientation for the endohedral unit is not sufficient to reproduce the experimental Dy-rXPD pattern. Also, is is not possible to clearly evidence or exlude a possible pyramidalization of the endohedral unit. However, two co-existing endohedral configurations – one with a planar unit inclined with respect to the (111) surface and a slightly pyramidal one approximately parallel to the surface – satisfactorily reproduce the experiment. The corresponding best-fit Dy-SSC calculation is shown in Fig. 4c (upper half). Also with this pattern that assumes endohedral Dy_3N units with different conformations, the agreement between simulation and experiment is not as good as for the N1s and C1s patterns with the R-factor being approximately 30% larger. Since an isotropic distribution of the endohedral atoms can be excluded (Figure 4c lower half) it can nevertheless be concluded that the endohedral unit adopts its orientation to the presence of the underlying surface, resulting in more than one co-existing orientations of the endohedral unit in the adsorbed state. This is in line with several co-existing orientations of the latter within co-crystals [5, 8, 25, 26].

With the large variety of currently available multi-atom endohedral fullerenes [27], the adsorption of such endohedral fullerenes on single crystal surfaces provides a means to create ordered arrays of endohedral, decoupled clusters which might be oriented by application of external fields. The present study has shown that monolayer-thick, ordered arrays of endohedral fullerenes can be grown and characterized on single-crystal surfaces, opening the way for future experiments exploring these ideas which would be relevant for nanoscale information storage.

In summary, we have shown that the endohedral fullerene $Dy_3N@C_{80}$ (I_h) adsorbs on Cu(111) in a way that at monolayer coverage, both the cage and the endohedral unit are ordered. The C_{80} cage faces towards the surface with a hexagon whose plane is slightly tilted with respect to the substrate. The look inside the endohedral fullerene indicates that the nitrogen remains at the center of the cage and the endohedral Dy_3 unit takes at least two inequivalent orientations with respect to the substrate surface.

Financial support from the Swiss National Science Foundation and the NCCR 'nanoscale science' is gratefully acknowledged. Part of these experiments were performed on the SIM beamline at the Swiss Light Source, Paul Scherrer Institut, Villigen, Switzerland.

References

[1] H. Shinohara, Rep. Prog. Phys. **63**, 843 (2000).

[2] S. Stevenson *et al.*, Nature **401**, 55 (1999).

[3] L. Dunsch *et al.*, J. Phys. Chem. Solids **65**, 309 (2004).

[4] L. Alvarez *et al.*, Phys. Rev. B **66**, 035107 (2002).

[5] S. Stevenson *et al.*, Chem. Commun., 2814 (2004).

[6] S. F. Yang, and L. Dunsch, Chem.-Eur. J. **12**, 413 (2006).

[7] M. Wolf *et al.*, Angew. Chem.-Int. Edit. **44**, 3306 (2005).

[8] S. F. Yang *et al.*, J. Am. Chem. Soc. **128**, 16733 (2006).

[9] M. Wolf *et al.*, J. Magn. Magn. Mater. **290**, 290 (2005).

[10] D. F. Leigh *et al.*, Surf. Sci. **601**, 2750 (2007).

[11] D. S. Deak *et al.*, J. Am. Chem. Soc. **128**, 13976 (2006).

[12] D. S. Deak *et al.*, Nanotechnology **18**, 6 (2007).

[13] C. Ton-That *et al.*, Phys. Rev. B **68**, 045424 (2003).

[14] R. A. J. Woolley *et al.*, Nano Lett. **4**, 361 (2004).

[15] I. Horcas *et al.*, Rev. Sci. Instrum. **78**, 013705 (2007).

[16] M. Treier *et al.*, Surf. Sci. **602**, L84 (2008).

[17] R. Fasel *et al.*, Phys. Rev. Lett. **76**, 4733 (1996).

[18] C. S. Fadley, in *Synchrotron Radiation Research: Advances in Surface Science*, edited by R. Z. Bachrach (Plenum, New York, 1990), pp. 421.

[19] R. Fasel *et al.*, Phys. Rev. B **50**, 14516 (1994).

[20] J. F. Moulder *et al.*, *Handbook of X-ray Photoelectron Spectroscopy* (Perkin-Elmer Corp., Eden Prairie, 1992).

[21] P. Kruger *et al.*, Surf. Sci. **601**, 3952 (2007).

[22] P. Kruger *et al.*, Phys. Rev. Lett. **100**, 055501 (2008).

[23] F. Bondino *et al.*, J. Phys. Chem. B **110**, 7289 (2006).

[24] A. Fohlisch *et al.*, Nature **436**, 373 (2005).

[25] S. Stevenson *et al.*, Inorg. Chem. **47**, 1420 (2008).

[26] S. Stevenson *et al.*, Chem.-Eur. J. **8**, 4528 (2002).

[27] L. Dunsch, and S. Yang, Small **3**, 1298 (2007).